



Mineralization and morphology of peri-implant bone around loaded and unloaded dental implants retrieved from the human mandible

Fausto Zamparini^{1,2} · Maria Giovanna Gandolfi¹ · Andrea Spinelli² · Mauro Ferri³ · Giovanna Iezzi⁴ · Daniele Botticelli⁵ · Carlo Prati²

Received: 19 May 2023 / Accepted: 12 August 2023
© The Author(s) 2023

Abstract

Purpose Limited data is reported regarding the bone mineralization around dental implants in the first months from insertion. The study analyzed the peri-implant bone around loaded and unloaded implants retrieved from human mandible after 4 months from placement.

Method The composition and mineralization of human bone were analyzed through an innovative protocol technique using Environmental-Scanning-Electron-Microscopy connected with Energy-Dispersive-X-Ray-Spectroscopy (ESEM/EDX). Two regions of interest (ROIs, approximately 750×500 μm) for each bone implant sample were analyzed at the cortical (Cortical ROI) and apical (Apical ROI) implant threads. Calcium, phosphorus, and nitrogen (atomic%) were determined using EDX, and the specific ratios (Ca/N, P/N, and Ca/P) were calculated as mineralization indices.

Results Eighteen implant biopsies from ten patients were analyzed (unloaded implants, $n=10$; loaded implants, $n=8$). For each ROI, four bone areas (defined bones 1–4) were detected. These areas were characterized by different mineralization degree, varied Ca, P and N content, and different ratios, and by specific grayscale intensity detectable by ESEM images. Bony tissue in contact with loaded implants at the cortical ROI showed a higher percentage of low mineralized bone (bone 1) and a lower percentage of remodeling bone (bone 2) when compared to unloaded implants. The percentage of highly mineralized bone (bone 3) was similar in all groups.

Conclusion Cortical and apical ROIs resulted in a puzzle of different bone “islands” characterized by various rates of mineralization. Only the loaded implants showed a high rate of mineralization in the cortical ROI.

Keywords Dental implants · ESEM-EDX · Retrieved implants · Peri-implant bone · Loading · Mineralization degree

✉ Fausto Zamparini
fausto.zamparini2@unibo.it

Maria Giovanna Gandolfi
mgiovanna.gandolfi@unibo.it

Andrea Spinelli
andrea.spinelli4@unibo.it

Mauro Ferri
medicina2000ctg@hotmail.com

Giovanna Iezzi
gio.iezzi@unich.it

Daniele Botticelli
daniele.botticelli@gmail.com

Carlo Prati
carlo.prati@unibo.it

¹ Laboratory of Biomaterials and Oral Pathology, Department of Biomedical and Neuromotor Sciences, School of Dentistry, University of Bologna, 40126 Bologna, Italy

² Endodontic Clinical Section, Department of Biomedical and Neuromotor Sciences, School of Dentistry, University of Bologna, 40126 Bologna, Italy

³ School of Dentistry, Corporación Universitaria Rafael Núñez, 130001 Cartagena, de Indias, Colombia

⁴ Department of Medical Oral and Biotechnological Sciences, University of Chieti/Pescara, 66013 Chieti, Italy

⁵ ARDEC Academy, 47923 Rimini, Italy

Introduction

Histological and biochemical investigations of peri-implant bone tissue indicate great cell turnover with different cells involved in neo-angiogenesis, vascularization, bone formation, and remodeling, which are responsible for new bone morphology [1–7].

Osseointegrated dental implants should possess thick and strict bone tissue around the subcrestal threads [4, 8]. For this reason, bone implant contact is usually calculated on histological samples [9–11]. Bone in contact with the implant surface and bone around the implant can be influenced by mechanical loads, particularly in the early months after insertion [4].

In recent years, different animal models have been used to study bone morphology around implants immediately after insertion and during bone healing [12–17]. However, animal models usually have discrepancies when directly translated to humans. In some studies, no occlusal load was applied to the implants [14–17]. In other studies, femoral or tibial bones were used, with obvious biological and biomechanical differences [12, 13, 18, 19].

Several studies have considered retrieved human dental implants as samples to obtain more information on the morphology of the bone around and in contact with the implant surface in clinical conditions [1–3, 5–7, 10, 20, 21]. These morphological studies demonstrated great remodeling activity with many modifications of bone and with an active role of the blood clot and other tissues [1–3, 5–7]. The roles of necrotic bone debris, smear layer, and fibrous tissue have only partially been described in these studies [3, 5, 20, 21]. Moreover, limited data is reported regarding the bone mineralization and composition around dental implants in the first months from their insertion in human mandible.

Environmental Scanning Electron Microscopy (ESEM) connected with Energy Dispersive X Ray Spectroscopy (EDX) allows to evaluate the element content (atomic %) of inorganic and organic samples. Recently, a protocol to investigate the bone mineralization around retrieved dental implants has been conceived [22, 23]. This analysis has been used to investigate the composition of bone around implants using histological preparations from human biopsies, providing a direct comparison with the optical information from the same histological preparation [22–25].

The aim of this study was to investigate the bone mineralization and morphology around dental implants retrieved from the human mandible after 4 months under two different loading conditions. One implant group was loaded after 2 months, and the other group was left unloaded.

Methods

Detailed information on the clinical procedures have been reported in a previous paper [5]. The protocol of the study was approved on October 8, 2014, (CURN 07- 2014) by the Ethical Committee of the Corporación Universitaria Rafael Núñez, Cartagena de Indias, Colombia.

Sample size calculation has been performed following a previous paper [26]. PS Power and Sample Size Calculations software (Version 3.0) was used [27]. In order to reach Power analysis 0.9 and α error 0.05, a minimum of 12 implants per group were necessary. This number was further increased to 16 to compensate for any losses or problems with biopsies analyses.

All procedures were made according to the recommendations of the declaration of Helsinki [28]. The study was designed in accordance with the CONSORT guidelines [29].

Healthy, nonsmoker volunteers were recruited and had to fulfill strict inclusion criteria [5]. Patients received two mini-implants (5-mm height, 3.5-mm width, Sweden & Martina, Due Carrare, Padova, Italy) in the posterior region of the mandible (molar areas). All surgeries were conducted on fully-healed crests in sites with adequate bone volumes and height and without the need for any bone graft procedures.

All implants were characterized by a ZirTi surface (Sweden & Martina, Due Carrare, Padova, Italy), obtained by zirconium microspheres sandblasting and by hydrofluoric acid, sulfuric acid, and hydrochloric acid etching treatments [30].

All surgical procedures were performed by a skilled operator. After local anesthesia, full-thickness flaps were raised, and an osteotomy performed with a series of drills with increasing diameter. Final alveolar socket preparation was 2.8 mm in width in the apical portion, 3.0 mm in width in the cortical portion, and 5.0 mm in depth. Implants were placed with the cortical margin flush to the bony crest. A healing screw was positioned to allow a non-submerged placement.

Implant loading protocol was selected according to Gallucci et al. [31]. After 2 months, each patient had one implant randomly loaded with a cement-retained crown (loaded group); the other implant was left unloaded (unloaded group). In loaded group, cemented resin crowns were inserted and maintained up to 4 months from placement. Crowns were designed only to have vertical contacts, which were checked at 3 months and 4 months from implant placement [5]. In the unloaded group, the healing screw was maintained up to 4 months from placement.

Histological biopsies preparation

Detailed information on the histological preparation has been reported in a previous paper [5]. After 4 months from installation, mini-implants were removed with a trephine

bur. Biopsy specimen containing the implants were fixed in 10% buffered formalin immediately after retrieval.

The specimens were first dehydrated in alcohol and then included in a glycol methacrylate resin (Technovit 7200 VLC; Kulzer, Wehrheim, Germany). Subsequently, they were polymerized and sectioned using a diamond steel disc along the major axis of the implants at approximately 150 mm and ground to about 30 μm . The sections were stained with acid fuchsin and toluidine blue.

Optical microscopy and ESEM-EDX microanalysis

Optical microscopy (OM) was used to identify the peri-implant bone morphology.

The biopsies were then placed on the ESEM stub and examined without any prior preparation (uncoated samples) following the previously-validated protocol set by Gandolfi et al. [22–25]. Operative parameters were established as follows: low vacuum 100 Pascal, accelerating voltage of 20–25 kV, working distance of 8.5 mm, and 133-eV resolution in Quadrant Back-Scattering Detector mode (0.5 wt% detection level, amplification time 100 μs , measuring time 60 s). All images were taken with the same parameters and at the same magnification on each implant ROI.

Two regions of interest (ROI) of $750 \times 500 \mu\text{m}$ were selected in correspondence to the first cortical (Cortical ROI) and the last apical thread (Apical ROI) with bone tissue (Fig. 1).

The mineral content was measured using EDX with ZAF correction in areas of approximately $30 \times 30 \mu\text{m}$, and the qualitative and semiquantitative element contents (weight % and atomic %) were evaluated. The presence of calcium (Ca), phosphorous (P), nitrogen (N), and relative atomic ratios (Ca/P, Ca/N, and P/N) were calculated for all spectra. EDX mapping was also performed to detect the elemental distribution of Ca, P, N, and C in the selected ROIs (Fig. 2).

In each ESEM image, areas with different gray intensities (electron densities) were identified. The value of gray intensity from dark to light was provided by the Image J software (NIH software, Bethesda, MD, USA) and used to set bone areas with different elemental concentrations and morphologies. Bone 1 corresponds to the lowest electron density (dark gray), and bone 4 corresponds to the highest electron density (light gray) (Fig. 2). EDX mapping was also performed to analyze the mineralization gradient (Fig. 2). The grayscale intensity was then correlated with the EDX data following a previous methodology [32] that was applied in other histological biopsy analyses [24, 25].

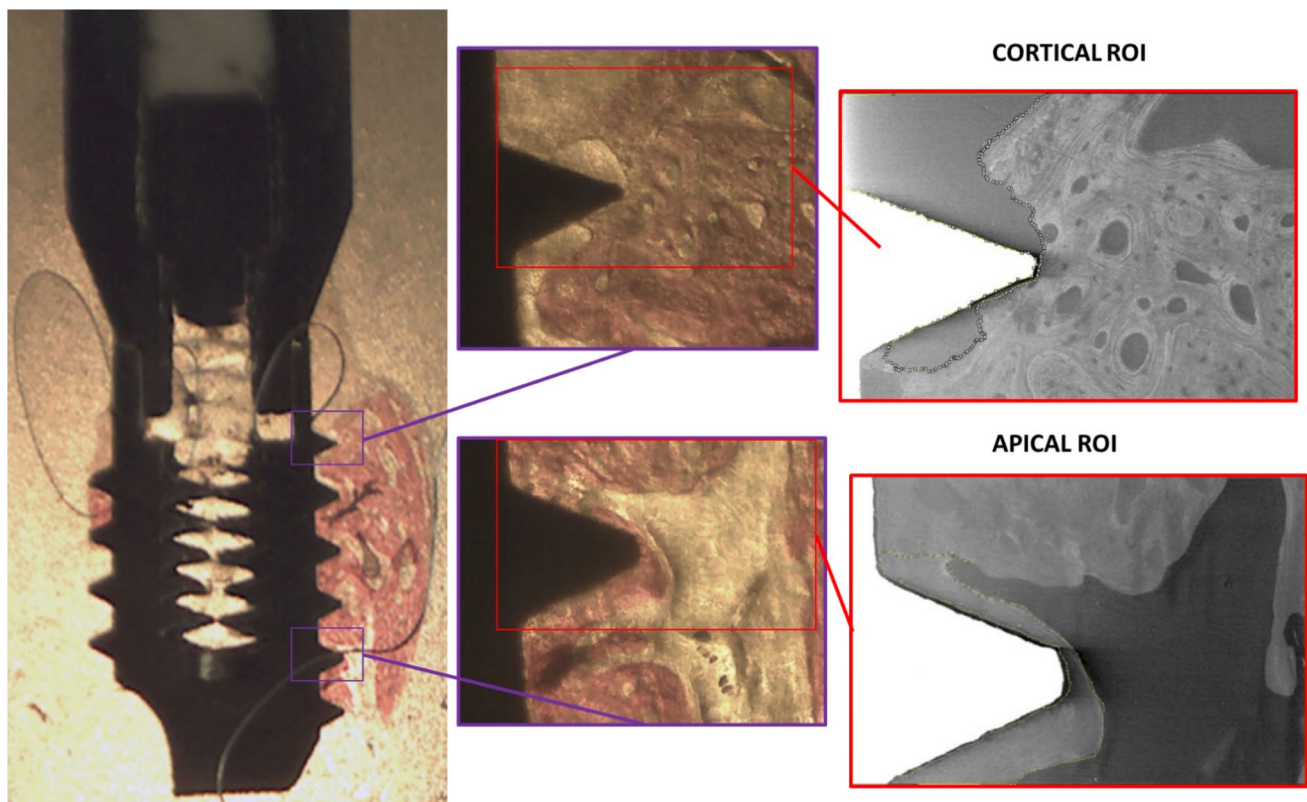
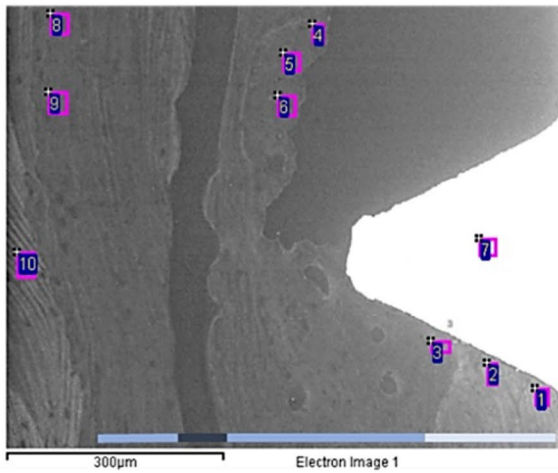


Fig. 1 Cortical and apical ROIs selection from a histological sample

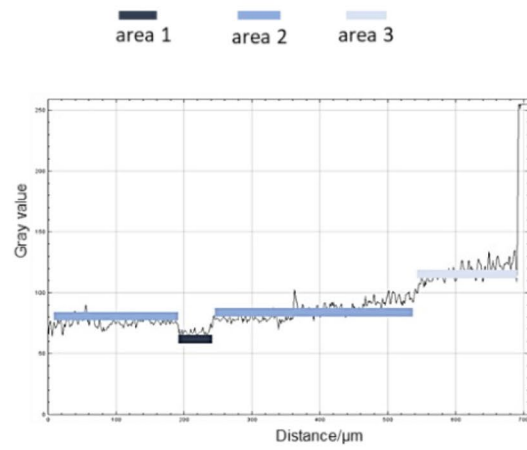
Optical Microscope



ESEM Image



Grayscale intensity quantification



EDX mapping

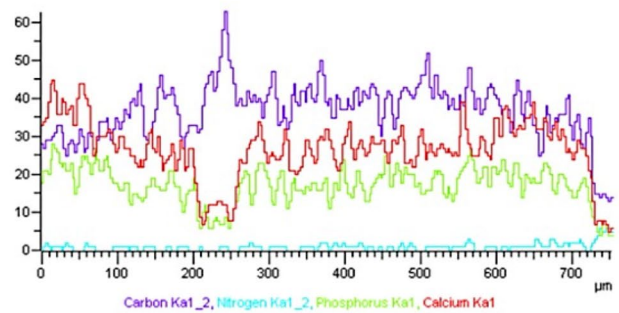
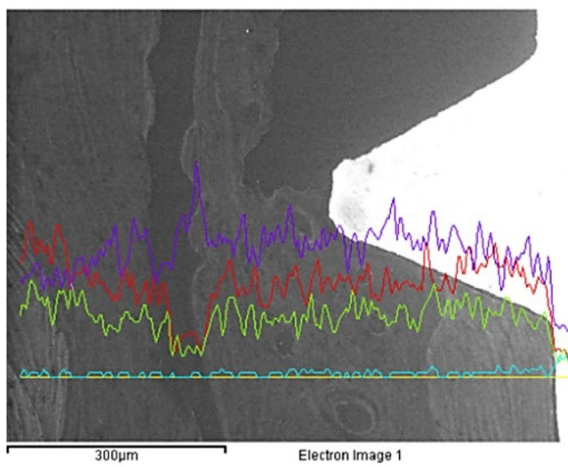


Fig. 2 Bone areas calibration performed on the biopsy of one unloaded implant. The area observed at OM (approx. 200× magnification) was analyzed through ESEM and EDX (500× magnification). Greyscale electron density values were then calculated on each image to determine grayscale threshold. Three different gray scale steps were identified on the analyzed area, each of these corresponded to an area with different gray intensity. These data were correlated to the semiquantitative EDX analysis of the mineral (Ca and P) and organic (N) content

The extension of different electron-dense bone areas was measured, and the scale bar provided by ESEM was used for ImageJ calibration. Three measurements were performed for each ROI and the mean values (μm^2) were recorded. For each ROI, the bone area percentage was calculated.

Analyses of distant bone areas were performed to assess mineralization of the mature cortical bone.

The following bone areas were identified through ESEM/EDX based on grayscale intensity and organic/inorganic ion content (Fig. 2):

- Bone 1: Low-electron-density areas. ESEM images appear as dark gray areas, indicating a low mineralized bone or bone marrow area characterized by low inorganic (Ca, P) and high organic (N) content.
- Bone 2: Medium-electron-density areas. ESEM images appeared as medium-gray areas with numerous lacunae. These areas were defined as remodeled bone, characterized by moderate inorganic (Ca, P) and organic content (N).
- Bone 3: High-electron-density areas. Highly mineralized areas with high Ca, P, and N. Light gray areas are defined as mature old bone and are characterized by high inorganic and low organic contents.
- Bone 4: High-electron-density areas. Highly mineralized areas with a dense and homogeneous structure with high Ca and P. Light gray with high Ca/N and P/N and Ca/P areas were defined as the cortical bone tissue (Table 1).

Statistical analysis

Statistical data were analyzed using SigmaPlot software (Systat Version 13.0, USA).

One-way ANOVA was performed to detect statistically significant differences in the atomic values content and ratios among the bone types. Two-way ANOVA followed by a Holm-Sidak test (normality test $p > 0.05$, equal variance test $p > 0.05$) was performed to detect statistically significant differences between loaded and unloaded biopsies in both coronal and apical ROIs. The p value was set at 0.05.

Results

Five patients were excluded from the study because of chikungunya viral infections. One patient was excluded due to biopsy damage during histological processing. Other two biopsies of loaded implants from two patients were not analyzed because of histological slide detachment. A total of 18 implant biopsies were analyzed: ten included one unloaded implant and eight included one loaded implant (Fig. 3). Two representative histological samples, one from unloaded and one from loaded group are depicted in Figure S1, Supplementary material.

OM and ESEM-EDX analysis of loaded implants

Representative OM and ESEM images of cortical and apical ROIs from one loaded implant are reported in Figs. 4 and 5 respectively. Bone areas division/identification is reported in Fig. 6.

At Cortical ROI, low mineralized area was generally observed close to the implant surface (bone 1). Medium mineralized areas were detected approx. 300 μm from the implant surface (bone 2). High electron dense areas (bone 3) were detected close to bone 2 and at the limits of Cortical ROI (approx. 500 to 750 μm from the implant surface).

At the apical ROI, low mineralized areas (bone 1) were uniformly distributed. Medium mineralized area (bone 2) was detected close to the implant surface, while highly mineralized areas were observed at the limits of the ROI (bone 3).

EDX spectra showed the mineral content of the different bone areas in the coronal and apical ROIs (Figs. 4 and 5).

OM and ESEM-EDX analysis of unloaded implants

Representative OM and ESEM images of one loaded implant cortical and apical ROIs are reported in Figs. 7 and 8 respectively. Bone areas division/identification is reported in Fig. 9.

At Cortical ROI, low electron dense areas (bone 1) were mostly detected in sites close to the implant surface, while medium electron dense areas (bone 2) were predominant close to the implant surface and at distant sites. High electron dense areas were mostly observed at sites over 500 μm from the implant surface.

At apical ROI, a higher presence of bone 1 was observed, with limited bones 2 and 3.

Bone areas distribution in the entire ROIs

The distribution of bone areas in the entire ROIs is reported in Fig. 8 and Table 2.

At Cortical ROI, loaded implants showed lower percentages of bone 1 (20.15 ± 7.77) and higher percentages

Table 1 EDX atomic values (mean±SD) of Ca, P and N, Ca/N, P/N, Ca/P on the analyzed bone. In the vertical column, significant differences (different letters, $p<0.05$) among bone types are indicated

	Ca	P	N	Ca/N	P/N	Ca/P
Bone 1 Dark gray	1.10±0.5a	0.85±0.4a	13.63±2.3a	0.07±0.05a	0.06±0.04a	1.18±0.03a
Bone 2 Medium gray	1.52±0.6b	1.21±0.5b	12.59±1.6a	0.13±0.06b	0.10±0.05b	1.25±0.03b
Bone 3 Light gray	2.32±0.9c	1.72±0.6c	10.08±1.5b	0.21±0.07c	0.15±0.05c	1.34±0.04c
Bone 4 Light gray	2.78±0.7d	2.50±0.5d	11.68±1.2b	0.24±0.06c	0.19±0.04d	1.45±0.07d

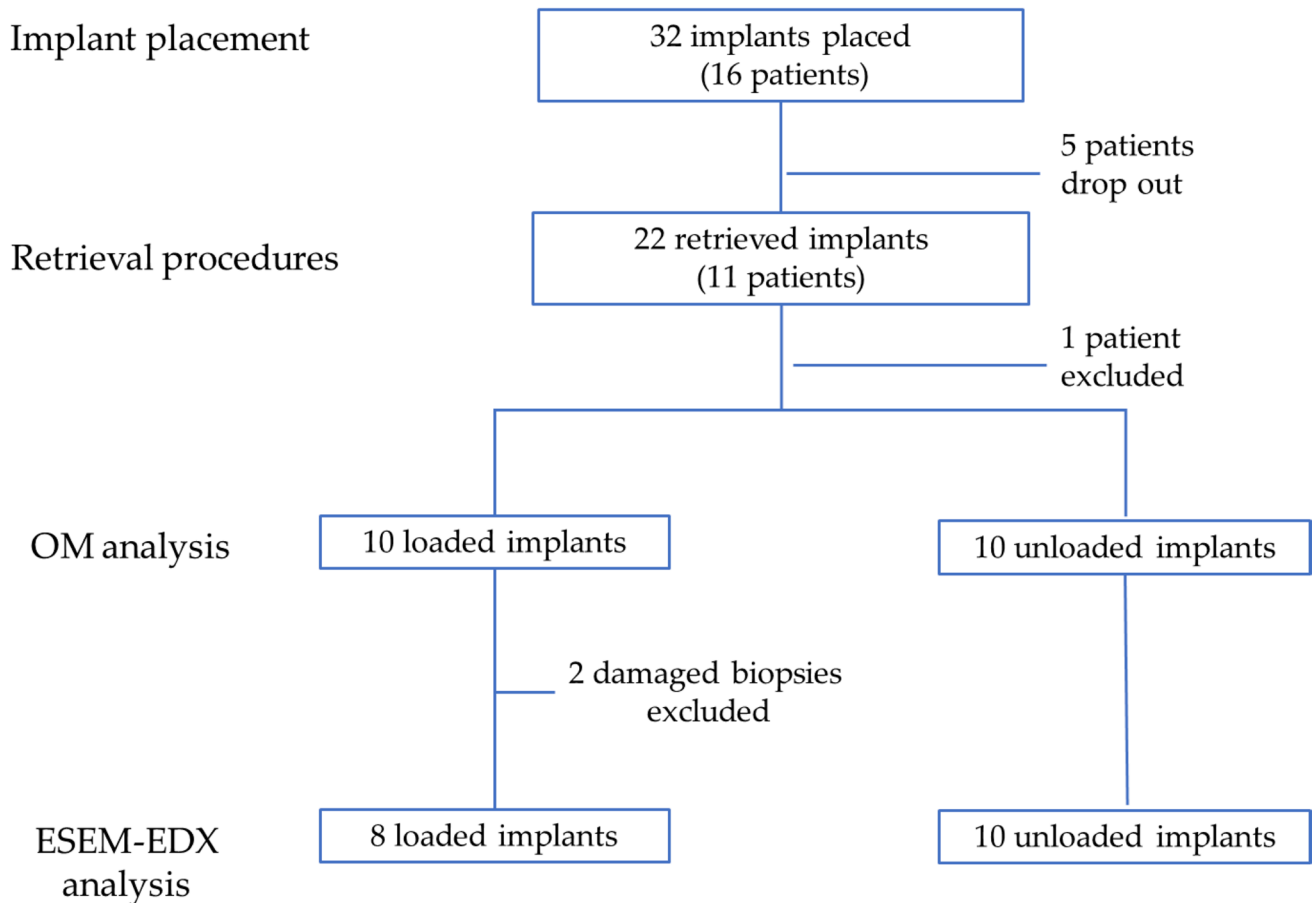


Fig. 3 Flowchart of the study. ESEM-EDX was performed on 18 implant biopsies, 8 comprising a loaded implant, 10 comprising an unloaded implant

of bone 2 (51.63 ± 12.02) when compared to unloaded implants (percentages of bones 1 and 2 were 35.6 ± 14.8 and 38.9 ± 11.1 respectively) (Table 2). Bone 3 showed similar values in both loaded and unloaded implants. This trend was observed also at the Apical ROI, where significantly lower percentages of bone 1 and higher percentages of bone 2 were detected in loaded implants (Fig. 10).

Bone 4 was not detected in cortical and apical ROI (Table 2). Only few samples of loaded group showed this bone area in distant sites from the cortical ROI (in 2/8 of cases).

Bone area distribution at peri-implant bone interface

The bone area distribution at peri-implant bone surface is reported in Table 2.

At cortical ROI, loaded implants had a high percentage of bone 1 (50.8 ± 17.4), moderate percentage of bone 2 (30.0 ± 12.65) and low presence of bone 3 (18.3 ± 12.1). This distribution is significantly different in the unloaded implants, where lower percentages of bone 1 (36.8 ± 15.8) ($p<0.05$) were detected at cortical ROI ($p<0.05$).

CORONAL ROI

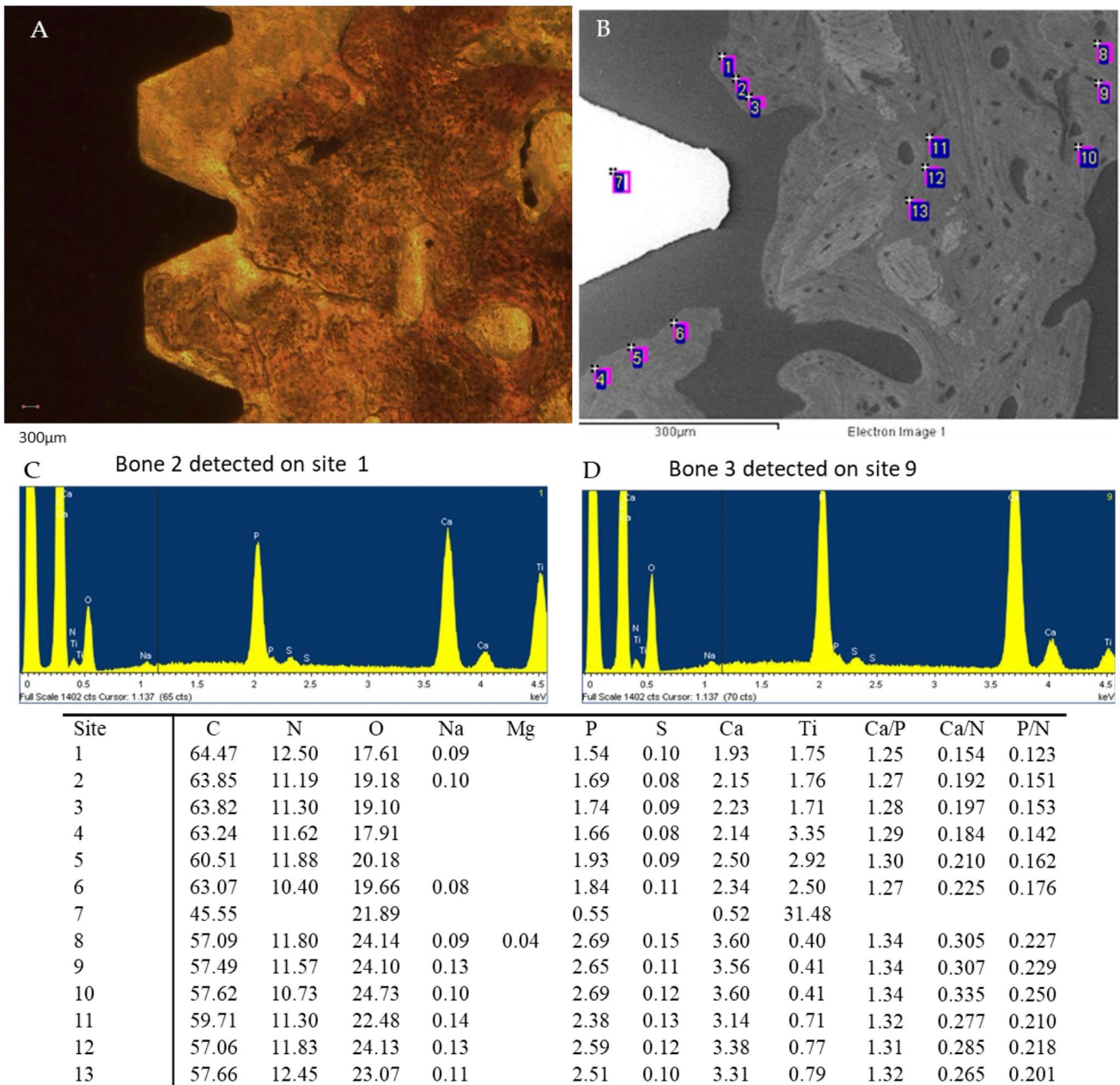


Fig. 4 Representative **A** OM and **B** ESEM images of one loaded implant. Scale bar (300 µm) is reported for comparison in both images. **E** EDX analysis performed on the ESEM-image. Values are

expressed as atomic percentages. Representative spectra of **C** bone 2 and **D** bone 3 are reported

At apical ROI, loaded implants showed low percentages of bone 1 (22.0±17.5), high percentage of bone 2 (65.0±16.5), and low percentages of bone 3 (13.0±11.8).

Apical surface of unloaded implants showed higher percentage of bone 1 (37.5±15.8), lower presence of bone 2 (50.1±12.0), and similar presence of bone 3 (13.4±8.6). No presence of bone 4 was detected at the interface in any cases.

Discussion

This study analyzed the bone tissues around loaded or unloaded human-retrieved implants and their level of tissue mineralization. It was focused on a portion of the peri-implant bone of approximately 500–700 µm of thickness, which was defined as the ROI. This region corresponded to the dimensions of the biopsy specimen.

APICAL ROI

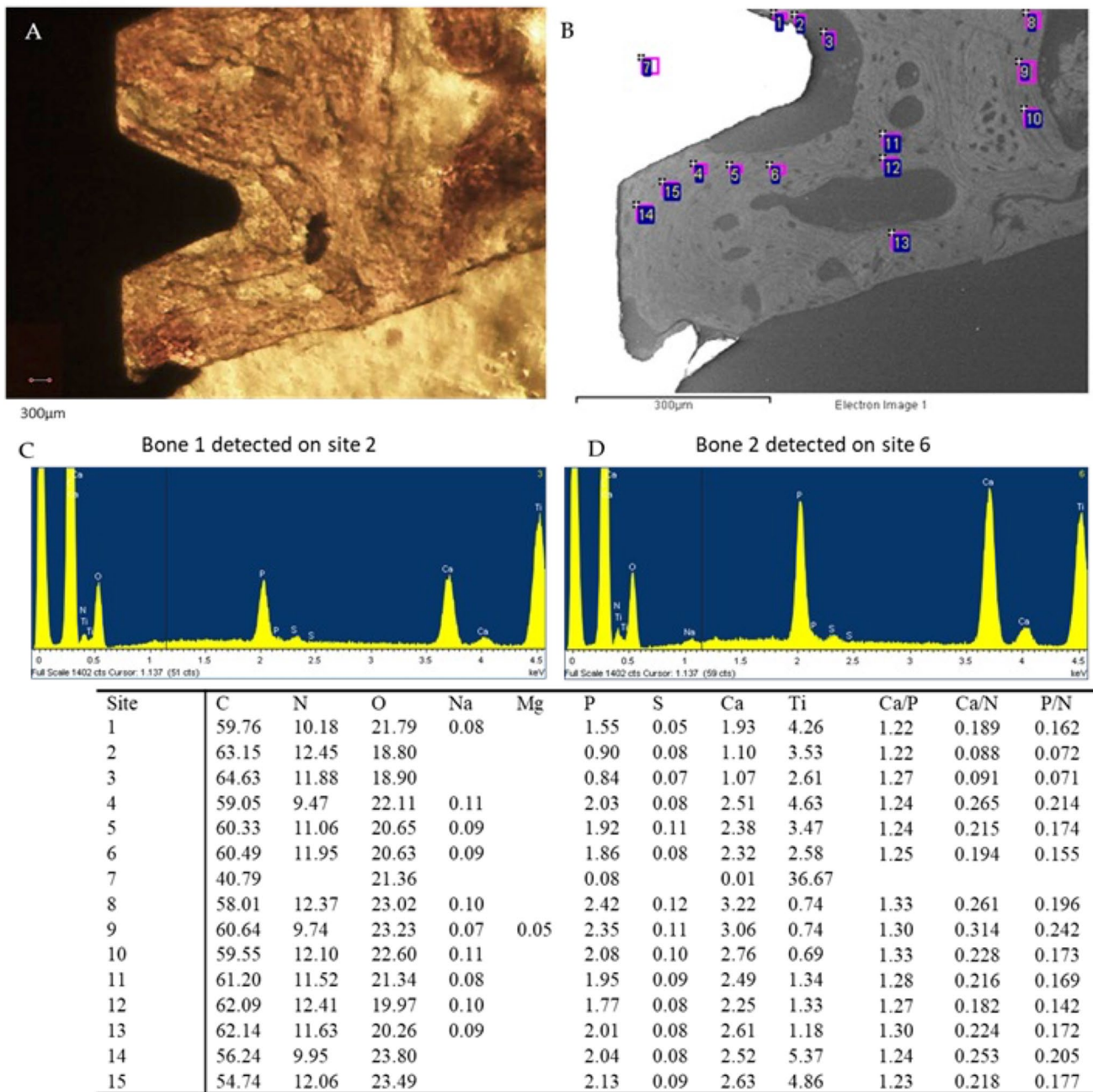


Fig. 5 Representative **A** OM and **B** ESEM images of one loaded implant Apical ROI. Scale bar (300 μm) is reported for comparison in both images. **E** EDX analysis performed on the ESEM-image. Values

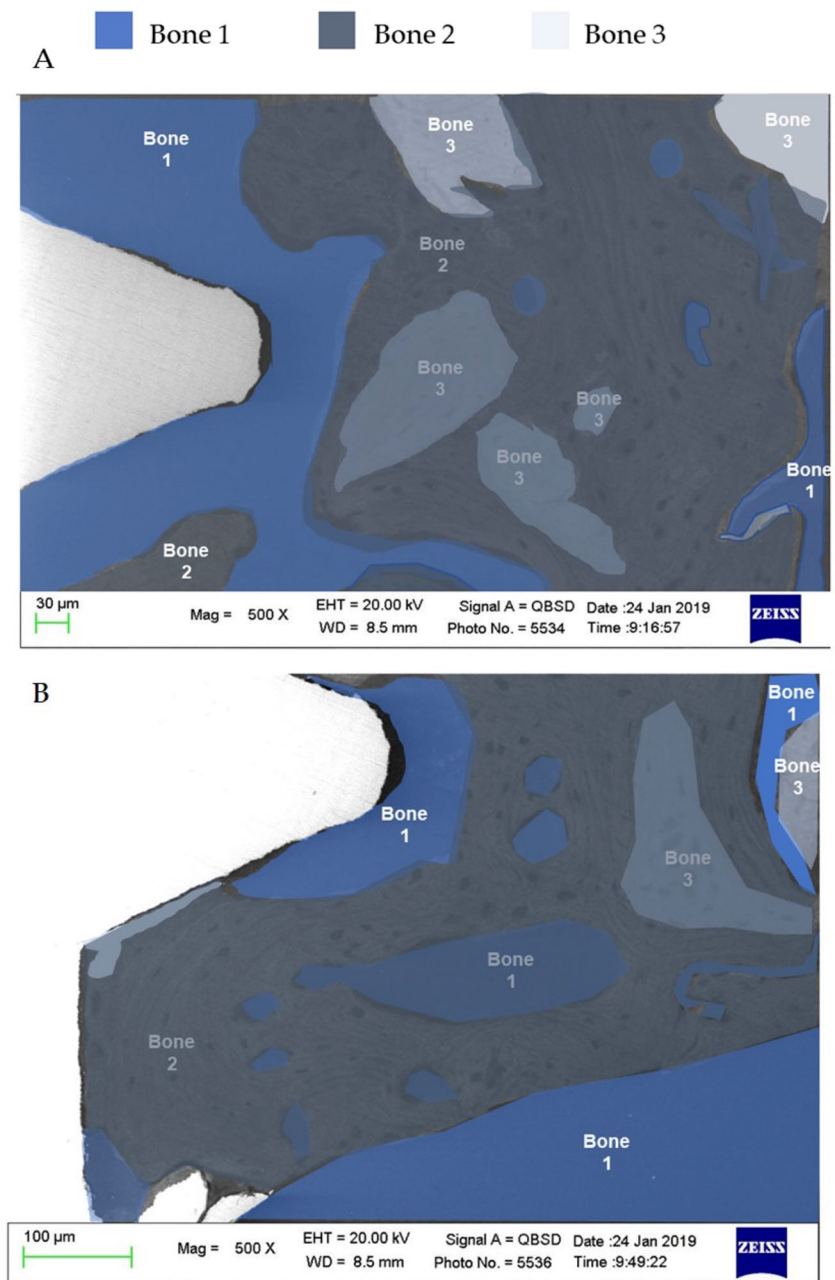
are expressed as atomic percentages. Please note the lower peaks of Ca and P in the spectra of **C** bone 1 when compared to **D** bone 2

The possibility of obtaining retrieved human biopsies and histological sample preparations allowed a “photography” of the morphological situation and mineral composition of bone 4 months after implant placement. The analysis was performed on histological samples using an ESEM connected to EDX [22, 23]. Mineralization analyses by

ESEM-EDX on bone histological biopsies has been innovatively proposed and validated by Gandolfi et al. for bone biomaterials in animal models [22] and for bone around retrieved implants in human [23–25].

The detection of different grayscale intensity areas (by ESEM) was associated with the calculation of organic (low

Fig. 6 Bone type classification in the selected **A** cortical and **B** apical ROI



z number elements, such as N) and inorganic (high z number elements, such as Ca and P) atomic percentages and ratios (by EDX) [22–25], allowing the creation of a map just around the implant (in the ROI) to compare with the morphological analyses previously performed by optical microscopy [24, 25].

This study identified different bone areas characterized by different levels of mineralization and different morphologies.

Bone architecture around the implant in the ROI underwent several modifications after the initial loading, in accordance with previous studies [12, 33–38].

In the selected ROIs, a dynamically active newly formed tissue was observed, which envelops and wraps all the implants creating a 400–700-µm thick nest/tissue. This tissue contained areas of moderate/high mineralization (bones 2 and 3, respectively) mixed with areas of low mineralization but rich in protein/collagen (bone 1), as

CORONAL ROI

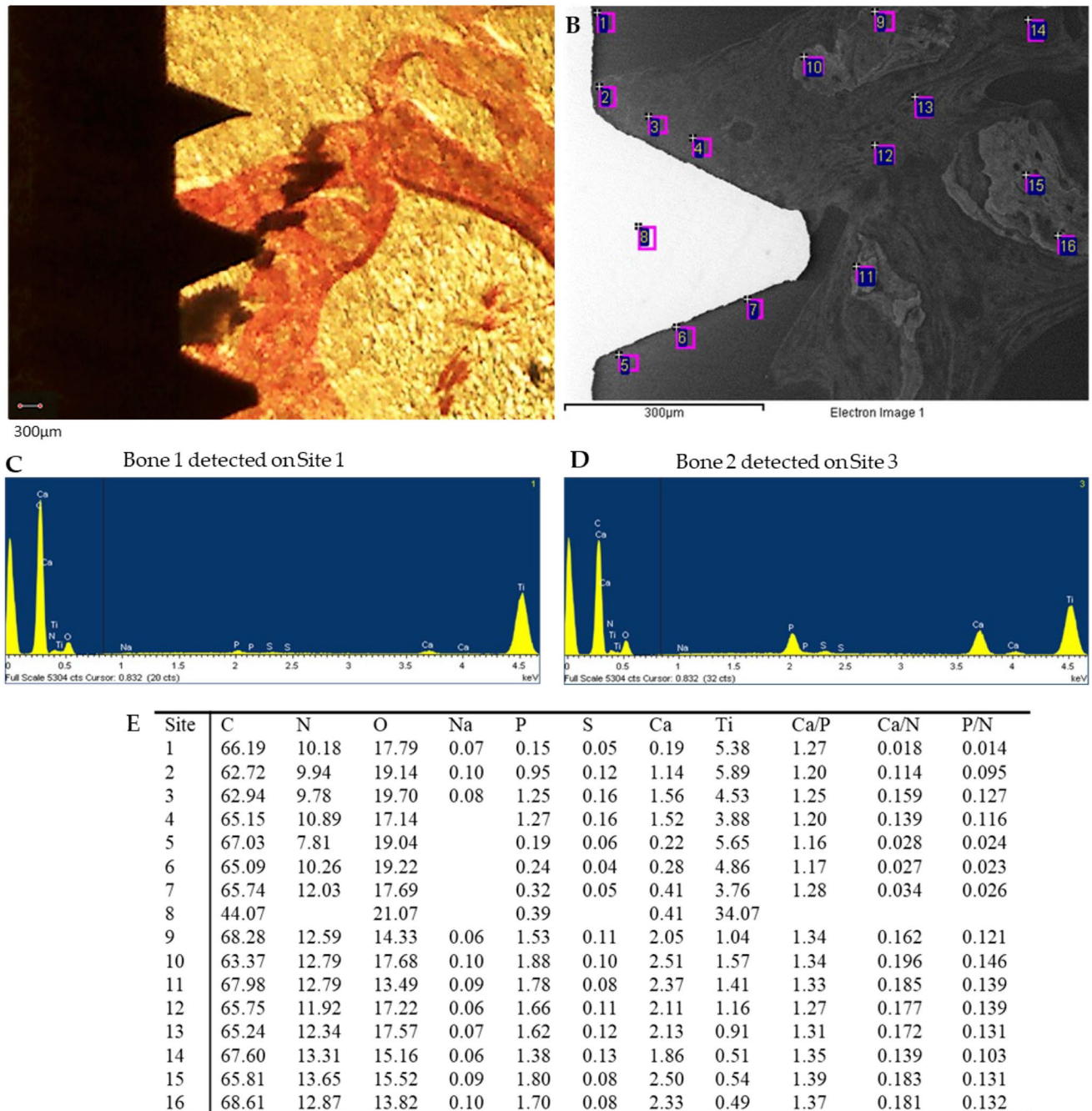


Fig. 7 Representative **A** OM and **B** ESEM images of 1 unloaded implant. Scale bar (300 μm) is reported for comparison in both images. **E** EDX analysis performed on the ESEM-image. Values are

expressed as atomic percentages. Please note the higher Ca and P peaks in the EDX spectra of **C** bone 3 when compared to (**D**) bone 1

demonstrated by the low Ca/N and P/N ratios. The low-mineralized areas showed high vascularization (detected by optical microscopy). In the periphery of ROIs, a dense mineralized bone was classified as bone 4 and probably represented the sound “old” bone not affected by the

biological modification induced by implant site preparation and implant placement.

The presence of different bone areas creates a puzzle that may well represent the active modification that takes part in the first months after placement [8, 35–41]. This

APICAL ROI

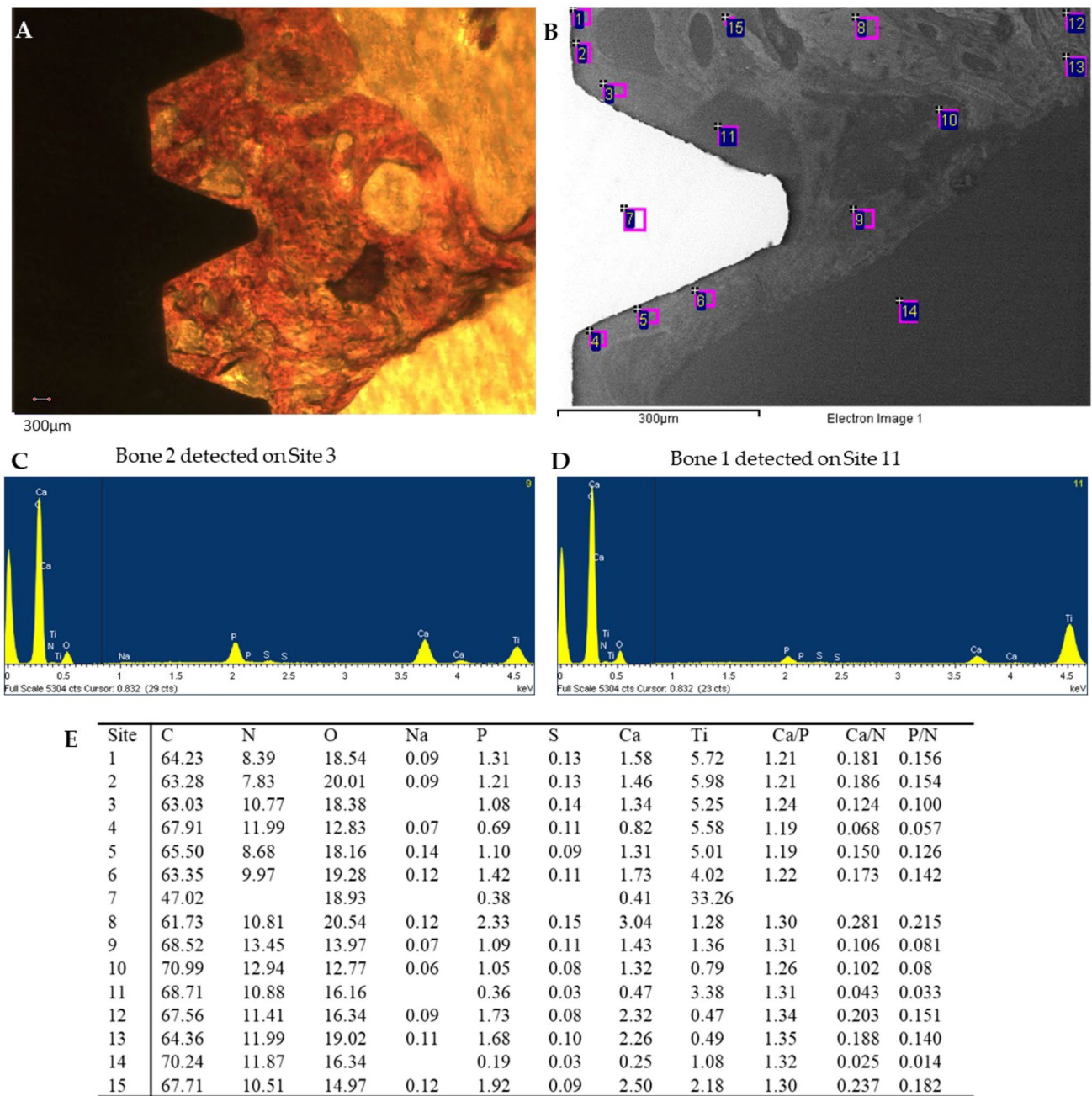


Fig. 8 Representative **A** OM and **B** ESEM images of 1 unloaded implant apical ROI. Scale bar (300 µm) is reported for comparison in both images. **E** EDX analysis performed on the ESEM-image. Val-

ues are expressed as atomic percentages. Please note the higher EDX peaks of Ca and P of C bone 2 when compared to D bone 1

bone structure is not far from the concept of honeycomb structure. The region around the implant (in this study, the ROI) contained different tissues with different elasticities and stiffnesses that can be compressed (and released) during mechanical repetitive loading. Accordingly, a recent study reported that the interface between the implant and bone is highly dynamic and “evolves” through a more

mineralized and stiff structure [42]. This is probably the biological reason for the different mineralized regions.

The study demonstrated that after 4 months, the presence of bones 3 and 4 at the cortical level was very modest and lower when considering the bone in contact with the implant interface. Bone 4, in particular, was detected only on distant sites from the investigated ROI and in a limited

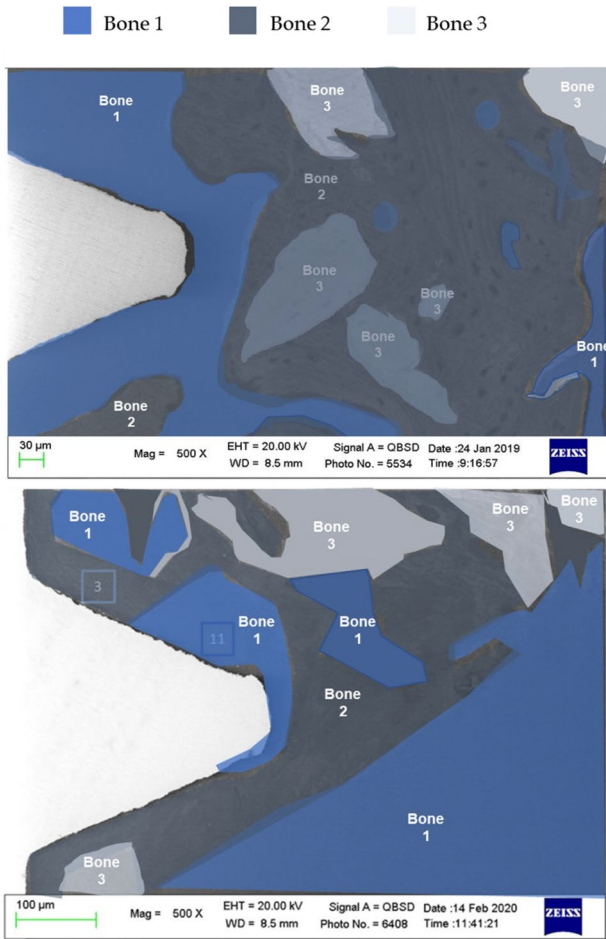


Fig. 9 Bone areas division/identification in the selected cortical and apical ROI of the unloaded implant

Table 2 Percentages of bone areas (mean± SD) measured at cortical ROI and apical ROI after 4 months from implant placement. In the horizontal row, significant differences (different letters, $p < 0.05$) among ROIs are indicated

	Loaded $n=8$		Unloaded $n=10$	
	Cortical ROI	Apical ROI	Cortical ROI	Apical ROI
Bone 1	20.1±7.8a	25.6±15.1a	35.6±14.8b	42.9±18.1b
Bone 2	51.6±12.0a	54.7±8.3a	38.9±11.1b	34.6±12.1b
Bone 3	28.2±11.1a	18.3±12.1a	25.1±10.3a	19.5±9.6a

number of specimens. New bone mineralization, formation of bones 2 and 3, started from the apical area and grew from deeper bone to superficial/cortical bone, contributing to the creation and maturation of cortical bone around the implant emergency. These findings suggests that the formation of a sound and complete cortical bone requires additional time.

The effect of implant loading on peri-implant bone was also analyzed in this study. Interestingly, a 2-month loading period induced a marked difference in terms of bone mineralization when compared with unloaded implants. The bone in strict contact with the implant surface showed interesting and unexpected results. In the cortical ROI, the unloaded group showed a larger percentage of bone 2 thighs with implant surface, while the loaded group had a higher percentage of bone 1, the less mineralized bone type.

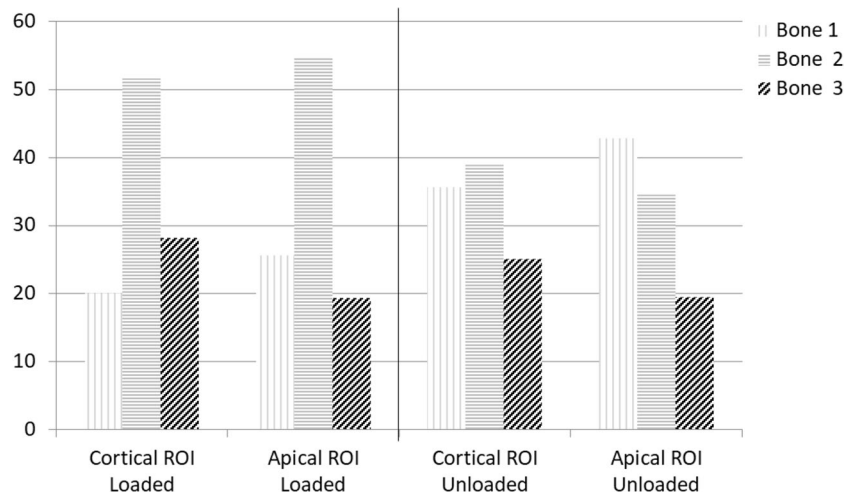
Implant loading induced the formation of a less mineralized but more elastic structure, represented by thin layers of low-mineralized bone structures that may reduce occlusal trauma and loading stress on healing tissue. During implant loading, the apical ROI underwent higher stress. In this way, the bone remodeling activities started from the most apical ROI and continued to the cortical ROI, which underwent fewer mechanical stimuli at the interface. A previous study reported that under physiological ranges (tolerated micromotion between 50 and 150 µm) [43], mechanical stimulation (i.e., loading) of implants decreases osteoclast activator signaling molecules (i.e., osteoprotegerin), leading to the differentiation of mesenchymal stem cells into osteoblasts and favoring new bone apposition [43]. Bone tissue acts as an elastic nest/chamber that can be deformed by loading, resulting in a reduced mineralized bone in contact with the cortical ROI [44].

The percentage of bone 3 (higher mineralization) in close contact with the implant surface was similar in both the groups. These percentages are probably sufficient to prevent dislocation and excessive movement of the implant.

The limitations of this study were the use of small-diameter implants. The dimensions of the implant were selected to allow easy removal of the implant with a limited residual bone defect [5]. The reduced dimension may be responsible for the observed bone morphology, as many studies have demonstrated that the greater the diameter, the lower the MBL [45, 46]. It should be highlighted that an early loading protocol was performed in the loading group. The loading protocol has been scientifically validated in a previous meta-analysis [31] but could lead to some discrepancies to the clinical practice, where definitive load is usually applied after 6 months.

The present results are not completely comparable with those reported by a previous histomorphometric study, which found only a slightly higher bone implant contact in loaded implants than in unloaded implants [5]. In the present study, only two different regions of interest were evaluated at the cortical and apical levels. Therefore, the percentage of bone in contact with the implant surface varied with previously published data that analyzed the entire bone implant contact.

Fig. 10 Bone areas distribution in loaded and unloaded implants at the selected ROIs. A high presence of bone 2 was observed in both cortical and apical ROIs. Differently, unloaded implants showed a higher presence of Bone 1



Conclusions

The study demonstrated that at least three different bone areas were identified on the basis of different mineralization levels and colors at ESEM in close contact with the implant surface and in the ROI. Four months after placement, the unloaded implants showed a more homogeneous distribution of bone 1, the less mineralized tissue, while the 2-month loaded implant showed more mineralized bone 2 in the ROI.

Supplementary Information The online version contains supplementary material available at <https://doi.org/10.1007/s10006-023-01175-1>.

Author contribution Authors Fausto Zamparini, Maria Giovanna Gandolfi, Andrea Spinelli, and Carlo Prati wrote the first draft of the manuscript; Authors Fausto Zamparini, Daniele Botticelli, and Carlo Prati wrote the final version of the manuscript; Mauro Ferri took care of the clinical study; Giovanna Iezzi took care of the histological processes; Fausto Zamparini and Andrea Spinelli performed the ESEM/EDX evaluation; Fausto Zamparini and Daniele Botticelli selected the images. All authors reviewed the manuscript.

Funding Open access funding provided by Alma Mater Studiorum - Università di Bologna within the CRUI-CARE Agreement. The clinical study was supported by ARDEC Academy, Rimini, Italy.

Data Availability Data are available on reasonable request.

Declarations

Ethical approval The protocol of the study was approved on October 8, 2014 (CURN 07- 2014) by the Ethical Committee of the Corporación Universitaria Rafael Núñez, Cartagena de Indias, Colombia.

Competing interests The authors declare no competing interests.

Open Access This article is licensed under a Creative Commons Attribution 4.0 International License, which permits use, sharing, adaptation, distribution and reproduction in any medium or format, as long as you give appropriate credit to the original author(s) and the source, provide a link to the Creative Commons licence, and indicate if changes were made. The images or other third party material in this article are

included in the article's Creative Commons licence, unless indicated otherwise in a credit line to the material. If material is not included in the article's Creative Commons licence and your intended use is not permitted by statutory regulation or exceeds the permitted use, you will need to obtain permission directly from the copyright holder. To view a copy of this licence, visit <http://creativecommons.org/licenses/by/4.0/>.

References

- Romanos GE, Johansson CB (2005) Immediate loading with complete implant-supported restorations in an edentulous heavy smoker: histologic and histomorphometric analyses. *Int J Oral Maxillofac Implants* 20:282–290
- Nevens M, Camelo M, Koo S, Lazzara RJ, Kim DM (2014) Human histologic assessment of a platform-switched osseointegrated dental implant. *Int J Periodontics Restorative Dent* 34:71–73
- Omori Y, Iezzi G, Perrotti V, Piattelli A, Ferri M, Nakajima Y, Botticelli D (2018) Influence of the buccal bone crest width on peri-implant hard and soft tissues dimensions: a histomorphometric study in humans. *Implant Dent* 27:415–423
- Bosshardt DD, Chappuis V, Buser D (2017) Osseointegration of titanium, titanium alloy and zirconia dental implants: current knowledge and open questions. *Periodontol* 2000(73):22–40
- Yonezawa D, Piattelli A, Favero R, Ferri M, Iezzi G, Botticelli D (2018) Bone healing at functionally loaded and unloaded screw-shaped implants supporting single crowns: a histomorphometric study in humans. *Int J Oral Maxillofac Implants* 33:181–187
- Imai H, Iezzi G, Piattelli A, Ferri M, Apaza Alccayhuaman KA, Botticelli D (2020) Influence of the dimensions of the antrostomy on osseointegration of mini-implants placed in the grafted region after sinus floor elevation: a randomized clinical trial. *Int J Oral Maxillofac Implants* 35:591–598
- Hirota A, Iezzi G, Piattelli A, Ferri M, Tanaka K, Apaza Alccayhuaman KA, Botticelli D (2020) Influence of the position of the antrostomy in sinus floor elevation on the healing of mini-implants: a randomized clinical trial. *J Oral Maxillofac Surg* 24:299–308. <https://doi.org/10.1007/s10006-020-00846-7>
- Albrektsson T, Wennerberg A (2019) On osseointegration in relation to implant surfaces. *Clin Implant Dent Relat Res* 21:4–7
- Piattelli A, Manzon L, Scarano A, Paolantonio M, Piattelli M (1998) Histologic and histomorphometric analysis of the bone

- response to machined and sandblasted titanium implants: an experimental study in rabbits. *Int J Oral Maxillofac Implants* 13:805–810
10. Mangano F, Mangano C, Piattelli A, Iezzi G (2017) Histological evidence of the osseointegration of fractured direct metal laser sintering implants retrieved after 5 years of function. *Biomed Res Int* 2017:9732136
 11. Botticelli D, Perrotti V, Piattelli A, Iezzi G (2019) Four stable and functioning dental implants retrieved for fracture after 14 and 17 years from the same patient: a histologic and histomorphometric report. *Int J Periodontics Restorative Dent* 39:83–88
 12. Romanos GE, Toh CG, Siar CH, Wicht H, Yacoob H, Nentwig GH (2003) Bone-implant interface around titanium implants under different loading conditions: a histomorphometrical analysis in the macaca fascicularis monkey. *J Periodontol* 2003(74):1483–1490
 13. Quaranta A, Iezzi G, Scarano A, Coelho PG, Voza I, Marincola M, Piattelli A (2010) A histomorphometric study of nanothickness and plasma-sprayed calcium-phosphorous-coated implant surfaces in rabbit bone. *J Periodontol* 81:556–561
 14. Cesaretti G, Lang NP, Salata LA, Schweikert MT, Gutierrez Hernandez ME, Botticelli D (2015) Sub-crestal positioning of implants results in higher bony crest resorption: a n experimental study in dogs. *Clin Oral Implants Res* 26:1355–1360
 15. Caroprese M, Lang NP, Rossi F, Ricci S, Favero R, Botticelli D (2017) Morphometric evaluation of the early stages of healing at cortical and marrow compartments at titanium implants: an experimental study in the dog. *Clin Oral Implants Res* 28:1030–1037
 16. Valles C, Rodríguez-Ciurana X, Nart J, Santos A, Galofre M, Tarnow D (2017) Influence of implant neck surface and placement depth on crestal bone changes around platform-switched implants: a clinical and radiographic study in dogs. *J Periodontol* 88:1200–1210
 17. Mainetti T, Lang NP, Bengazi F, Sbricoli L, Soto Cantero L, Botticelli D (2015) Immediate loading of implants installed in a healed alveolar bony ridge or immediately after tooth extraction: an experimental study in dogs. *Clin Oral Implants Res* 26:435–441
 18. Franchi M, Bacchelli B, Martini D, Pasquale VD, Orsini E, Ottani V, Fini M, Giavaresi G, Giardino R, Ruggeri A (2004) Early detachment of titanium particles from various different surfaces of endosseous dental implants. *Biomaterials* 25:2239–2246
 19. Franchi M, Fini M, Martini D, Orsini E, Leonardi L, Ruggeri A, Giavaresi G, Ottani V (2005) Biological fixation of endosseous implants. *Micron* 36:665–671
 20. Iezzi G, Degidi M, Shibli JA, Vantaggiato G, Piattelli A, Perrotti V (2013) Bone response to dental implants after a 3- to 10-year loading period: a histologic and histomorphometric report of four cases. *Int J Periodontics Restorative Dent* 33:755–761
 21. Iezzi G, Piattelli A, Mangano C, Degidi M, Testori T, Vantaggiato G, Fiera E, Frosecchi M, Floris P, Perroni R, Ravera L, Moreno GG, De Martinis E, Perrotti V (2016) Periimplant bone response in human-retrieved, clinically stable, successful, and functioning dental implants after a long-term loading period: a report of 17 CASES From 4 to 20 years. *Impl Dent* 25:380–386
 22. Gandolfi MG, Iezzi G, Piattelli A, Prati C, Scarano A (2017) Osteoinductive potential and bone-bonding ability of ProRoot MTA, MTA plus and biodentine in rabbit intramedullary model: microchemical characterization and histological analysis. *Dent Mat* 33:233–238
 23. Gandolfi MG, Zamparini F, Iezzi G, Degidi M, Botticelli D, Piattelli A, Prati C (2018) Microchemical and micromorphologic ESEM-EDX analysis of bone mineralization at the thread interface in human dental implants retrieved for mechanical complications after 2 months to 17 years. *Int J Periodontics Restorative Dent* 38:431–441
 24. Prati C, Zamparini F, Botticelli D, Ferri M, Yonezawa D, Piattelli A, Gandolfi MG (2020) The use of ESEM-EDX as an innovative tool to analyze the mineral structure of peri-implant human bone. *Materials* 13:1–13. <https://doi.org/10.3390/ma13071671>
 25. Romanos G, Zamparini F, Spinelli A, Prati C, Gandolfi MG (2022) ESEM-EDX microanalysis at bone-implant region on immediately loaded implants retrieved postmortem. *Int J Oral Maxillofac Implants* 37:51–60
 26. Rea M, Botticelli D, Ricci S, Soldini C, González GG, Lang NP (2015) Influence of immediate loading on healing of implants installed with different insertion torques—an experimental study in dogs. *Clin Oral Implants Res* 26:90–95. <https://doi.org/10.1111/clr.12305>
 27. Dupont WD, Plummer WD (1998) Power and sample size calculations for studies involving linear regression. *Control Clin Trials* 19:589–601
 28. World Medical Association (2013) World Medical Association Declaration of Helsinki: ethical principles for medical research involving human subjects. *J Am Med Assoc* 310:2191–2194
 29. von Elm E, Altman DG, Egger M, Pocock SJ, Gøtzsche PC, Vandenbroucke JP, & STROBE Initiative (2007) Strengthening the Reporting of Observational Studies in Epidemiology (STROBE) statement: guidelines for reporting observational studies. *BMJ* 335,806–808
 30. Caneva M, Lang NP, Calvo Guirado JL, Spriano S, Iezzi G, Botticelli D (2015) Bone healing at bicortically installed implants with different surface configurations. An experimental study in rabbits. *Clin Oral Implants Res* 26:293–299. <https://doi.org/10.1111/clr.12475>
 31. Gallucci GO, Hamilton A, Zhou W, Buser D, Chen S (2018) Implant placement and loading protocols in partially edentulous patients: a systematic review. *Clin Oral Implants Res* 29:106–134
 32. Roschger P, Fratzl P, Eschberger J, Klaushofer K (1998) Validation of quantitative backscattered electron imaging for the measurement of mineral density distribution in human bone biopsies. *Bone* 24:319–326
 33. Rocci A, Martignoni M, Burgos PM, Gottlow J, Sennerby L (2003) Histology of retrieved immediately and early loaded oxidized implants: light microscopic observations after 5 to 9 months of loading in the posterior mandible. *Clin Implant Dent Relat Res* 1:88–98. <https://doi.org/10.1111/j.1708-8208.2003.tb00020.x>
 34. Abrahamsson I, Berglundh T, Linder E, Lang NP, Lindhe J (2004) Early bone formation adjacent to rough and turned endosseous implant surfaces. An experimental study in the dog. *Clin Oral Implants Res* 15:381–392. <https://doi.org/10.1111/j.1600-0501.2004.01082.x>
 35. Berglundh T, Abrahamsson I, Lindhe J (2005) Bone reactions to longstanding functional load at implants: an experimental study in dogs. *J Clin Periodontol* 32:925–932. <https://doi.org/10.1111/j.1600-051X.2005.00747.x>
 36. Rossi F, Lang NP, De Santis E, Morelli F, Favero G, Botticelli D (2014) Bone-healing pattern at the surface of titanium implants: an experimental study in the dog. *Clin Oral Implants Res* 25:124–131

37. Shah FA, Ruscsák K, Palmquist A (2019) 50 years of scanning electron microscopy of bone—a comprehensive overview of the important discoveries made and insights gained into bone material properties in health, disease, and taphonomy. *Bone Res* 22:7–15. <https://doi.org/10.1038/s41413-019-0053-z>
38. Shah FA, Thomsen P, Palmquist A (2019) Osseointegration and current interpretations of the bone-implant interface. *Acta Biomater* 84:1–15
39. Albrektsson T, Johansson C (2001) Osteoinduction, osteoconduction and osseointegration. *Eur Spine J* 10:96–101. <https://doi.org/10.1007/s005860100282>
40. Davies JE (2003) Understanding peri-implant endosseous healing. *J Dent Educ* 67:932–949
41. Botticelli D, Lang NP (2017) Dynamics of osseointegration in various human and animal models - a comparative analysis. *Clin Oral Implants Res* 28:742–748
42. Xie J, Rittel D, Shemtov-Yona K, Shah FA, Palmquist A (2021) A stochastic micro to macro mechanical model for the evolution of bone-implant interface stiffness. *Acta Biomater* 131:415–423
43. Szmukler-Moncler S, Salama H, Reingewirtz Y, Dubruille JH (1998) Timing of loading and effect of micromotion on bone-dental implant interface: review of experimental literature. *J Biomed Mater Res* 43:192–203
44. Irandoust S, Müftü S (2020) The interplay between bone healing and remodeling around dental implants. *Sci Rep* 10:4335. <https://doi.org/10.1038/s41598-020-60735-7>
45. Telles LH, Portella FF, Rivaldo EG (2019) Longevity and marginal bone loss of narrow-diameter implants supporting single crowns: a systematic review. *PLoS One* 14:e0225046. <https://doi.org/10.1371/journal.pone.0225046>
46. Spinelli A, Zamparini F, Romanos G, Gandolfi MG, Prati C (2023) Tissue-level laser-look implants placed with a flapless technique: a 4-year clinical study. *Materials* 16(3):1293–1316. <https://doi.org/10.3390/ma16031293>

Publisher's note Springer Nature remains neutral with regard to jurisdictional claims in published maps and institutional affiliations.